

# Peptide Classification from Statistical Analysis of Nanopore Translocation Experiments

Julian Hoßbach,<sup>†,¶</sup> Samuel Tovey,<sup>†,¶</sup> Tobias Ensslen,<sup>‡</sup> Jan C. Behrends,<sup>‡</sup> and  
Christian Holm<sup>\*,†</sup>

<sup>†</sup>*Institute for Computational Physics, University of Stuttgart, 70569 Stuttgart, Germany*

<sup>‡</sup>*Laboratory for Membrane Physiology and Technology, Department of Physiology, Faculty  
of Medicine, University of Freiburg, 79104 Freiburg, Germany.*

<sup>¶</sup>*Equal Contribution*

E-mail: holm@icp.uni-stuttgart.de

## Abstract

Protein characterization using nanopore-based devices promises to be a breakthrough method in basic research, diagnostics, and analytics. Current research includes the use of machine learning to achieve this task. In this work, a comprehensive statistical analysis of nanopore current signals is performed and demonstrated to be sufficient for classifying up to 42 peptides with over 70 % accuracy. Two sets of features, the statistical moments and the *catch22* set, are compared both in their representations and after training small classifier neural networks. We demonstrate that complex features of the events, captured in both the *catch22* set and the central moments, are key in classifying peptides with otherwise similar mean currents. These results highlight the efficacy of purely statistical analysis of nanopore data and suggest a path forward for more sophisticated classification techniques.

# Keywords

Peptide characterization, Nanopore translocation, Machine learning

## Introduction

In the last decade, nanopore technology has emerged as a promising approach to third-generation DNA sequencing. In nanopore sensing, an analyte is driven through a nanoscale pore while a current is measured between the entrance and the exit<sup>1</sup>. The presence of the analyte inside the pore leads to a drop in the current that, ideally, is characteristic of the analyte present, making it suitable for analyte characterization. With its ability to produce long continuous reads in real-time and at low cost, the method has found a foothold in many areas of biomedicine, such as disease monitoring<sup>2,3</sup>, human genome research<sup>4</sup> and tumour detection<sup>5</sup>. Inspired by these successes, research has now begun to tackle the task of nanopore-based protein sensing in the rapidly growing field of proteomics, which would greatly benefit from new technology for efficient proteome exploration.

A peptide is defined as a chain of covalently bonded amino acids<sup>6</sup>, which, if large enough, is considered a protein. During this work, we are interested in classifying peptides. Classification, differs, however, to the sequencing often discussed in DNA. DNA sequencing is made possible through the use of DNA polymerase, a substance that ratchets DNA through a pore one base pair at a time, thus allowing for a controlled readout of the sequence. This approach is well established, and commercial solutions are available<sup>1</sup>. Machine learning has been applied extensively in improving the accuracy of these readouts<sup>7-11</sup>. However, such a mechanism is yet to be found in the case of peptides. Instead, current research focuses on classifying the entire analyte as it moves into the pore. Classification of peptides is of great interest to the medical community, in particular the identification of post-translational modifications, which have been shown to, among other things, indicate the presence of certain cancers<sup>12-15</sup>.

Several challenges underscore the complexity of nanopore-based peptide classification in comparison to DNA sequencing, among other things arising from a greater number of building blocks (amino acids) that constitute peptides. This makes sequencing based on current signals more complex, albeit in principle possible for the discrimination on a single amino acid<sup>16</sup>, or the detection of post-translational modifications<sup>17,18</sup>. Recent studies demonstrated that aerolysin nanopores are also suitable for protein fingerprinting based on the different blocking currents of the peptide fragments of cleaved proteins<sup>19</sup>. As the peptide enters the pore, the current is reduced depending on the geometry of the polymer entering along with its interactions between the solvent, itself, and the pore walls. As this blockage current depends on the geometry and interactions of the peptide, it can also be used to identify it. While this process is highly non-trivial, it does offer a pathway for classifying these peptide fragments and, perhaps, eventually, entire proteins. Similar reasoning has been used in work to predict properties of peptides based on the amino acid sequence and the structure of the peptide<sup>20</sup>. In this work, however, we investigate the readouts of 42 distinct peptides driven through a wild-type aerolysin nanopore<sup>21</sup> to determine what methods can be used to classify them.

We explore using the statistical moments of the distributions formed by individual pore-entry events and more advanced statistical measures to build a representation of the events and use these representations to train simple neural network classifiers. High-order moments of the distributions and time correlations in the signals are key in differentiating peptides with similar mean-blocking currents. This work demonstrates that the classification of large numbers of peptides in a single sample is possible, paving the way for applications eventually in pathology or, in the near term, aiding scientists performing peptide-nanopore experiments.

# Results and Discussion

## Feature Extraction

Starting from the current measurement, resulting in a time-series signal, as seen in Figure 1(a), we perform an event detection, followed by a normalization with respect to the open pore current, as discussed in the methods section. To illustrate that there are differences in the statistics of the resulting events of different peptides, we concatenate the normalized currents of all events of the peptides L3AA5, L4AA4 and L1AA8 into one continuous current signal and produce a histogram, respectively. Overlaying the resulting histograms by centering each peak around zero, one can identify differences in the width as well as other structural differences in the distribution, as illustrated in Figure 1(b). We aim to extract these differences in order to identify the individual peptides by their events by using two methods, which generate a fixed number of features of a time series to be used as feature vectors: The set of the first 10 central moments, which will be called the moment decomposition set, and the catch22 feature set<sup>22</sup>. Details on each feature set can be found in the methods section.

Before exploring the use of sophisticated classification algorithms for this, we perform a dimensionality reduction on the feature vectors to determine whether any structure can be found without additional processing. Figures 2(a) and 2(b) show a t-distributed Stochastic Neighbor Embedding (t-SNE)<sup>23</sup> as implemented in the scikit-learn<sup>24</sup> (Additional t-SNE plots with varying parameters can be found in Figures 1 and 2 in the supplementary information.). T-SNE embeds data from higher dimensions into lower dimensions while retaining their structure as much as possible. This means that similar points in high-dimensional space will be mapped closer together in low-dimensional space. It is a valuable tool for understanding structure in otherwise hard-to-visualize datasets. In the ideal case, t-SNE embedding would represent the data from each featurization process into N distinct clusters for N classes, i.e. 42 in this work, each representing an individual peptide. The datasets have a structure in

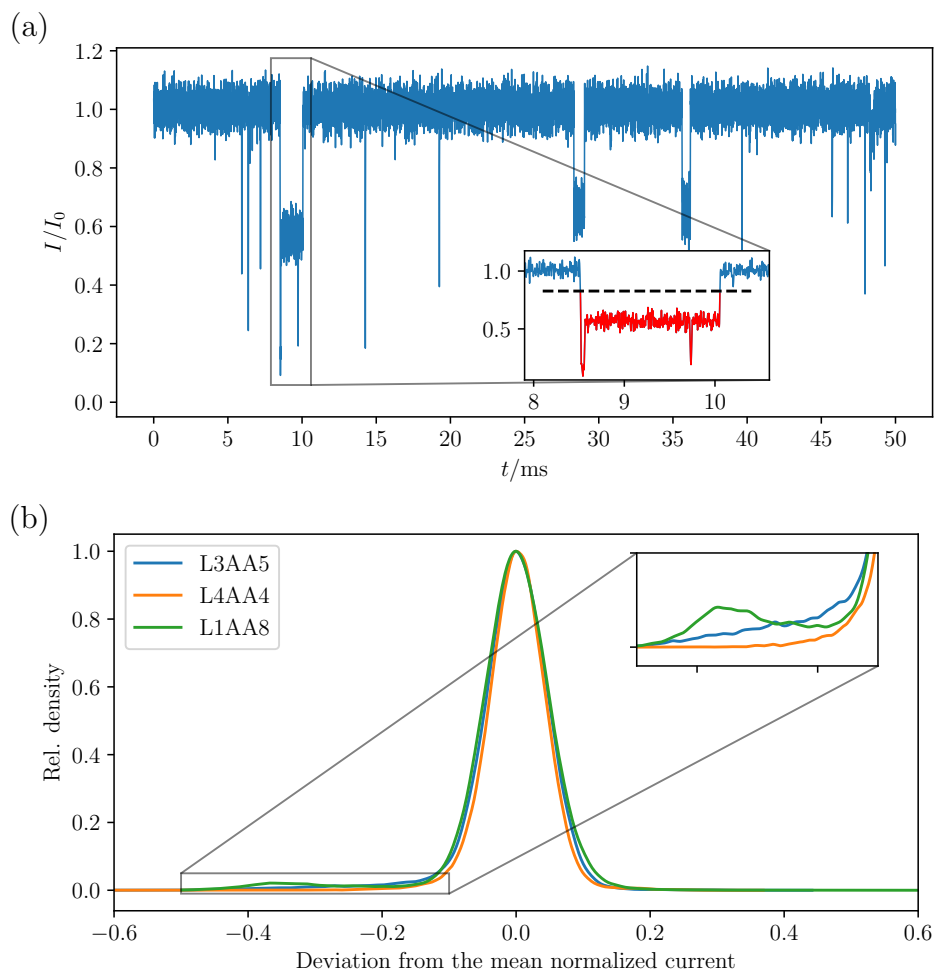


Figure 1: (a) Example of a normalized current readout with several events visible. The dashed line in the inset shows the cutoff, below which events are detected. The event current is shown in red. Details on the event detection and normalization are found in the methods section. (b) Histogram of the continuous signal of all events for the peptides L3AA5, L4AA4 and L1AA8. Each peak is shifted to be centered around 0 in order to visualize differences in the tails.

both the moment decomposition and the catch22 feature extraction. However, these clusters are not clear enough to identify 42 distinct classes. Therefore, more advanced classification means must be used to distinguish events further.

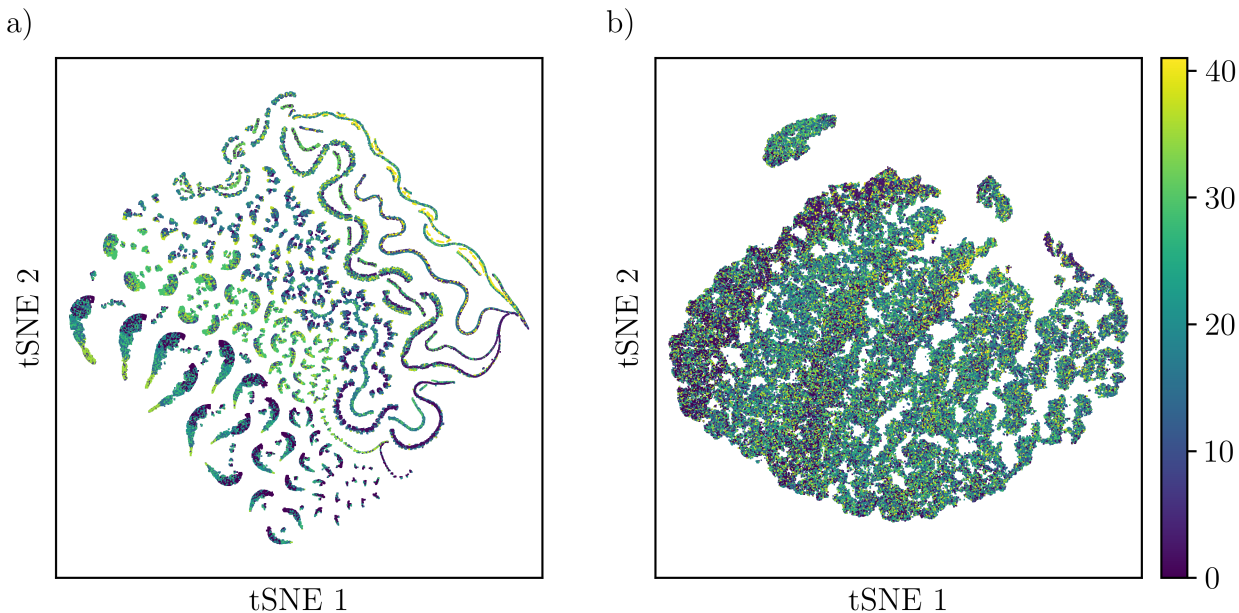


Figure 2: t-SNE embedding of the two feature extraction methods studied here, moment decomposition (a) and catch22 (b). Color represents the respective class associated with the coordinate. It is clear from the t-SNE plots that some structure is present in the vector representations. However, it is not enough to make accurate statements regarding classification.

## Model training

The previous investigation established that the two statistical means of converting the pore-entry events into feature vectors yield a representation with intrinsic structure. However, this structure alone is insufficient to separate classes; therefore, a more sophisticated means of classification is applied using the feature vectors as inputs, namely, feed-forward neural networks. Further information regarding the network training can be found in the methods section. Figure 3 shows the results of training neural networks on the moment decomposition and catch22 data sets. In Figure 3, the confusion matrices from the moment decomposition and catch22 trained models, respectively, are shown. The confusion matrices provide an

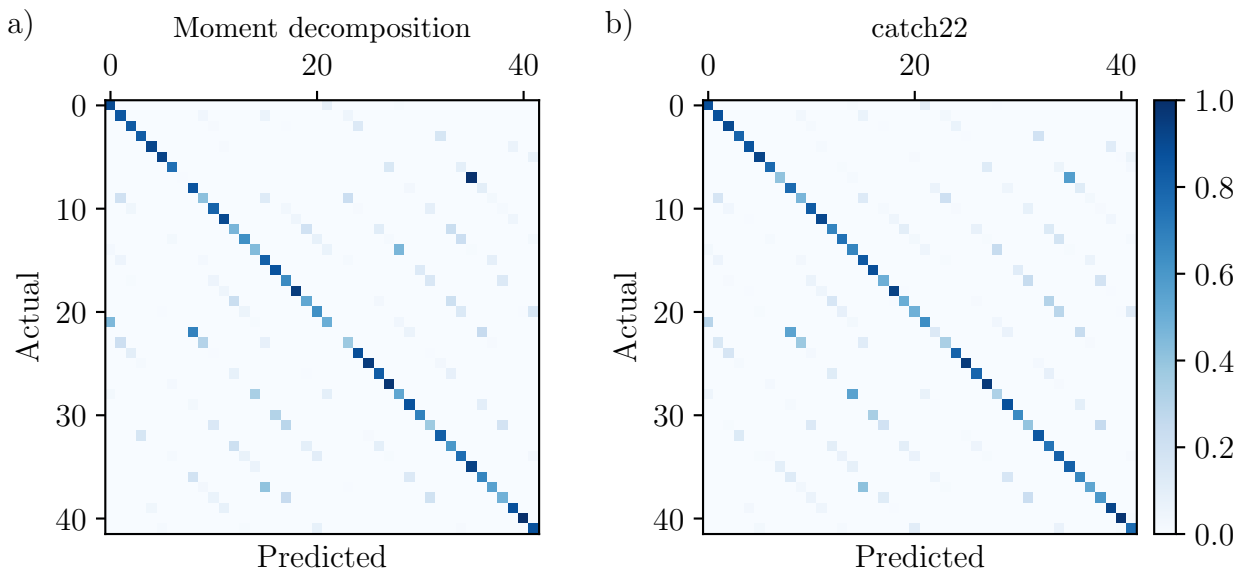


Figure 3: (a-b) Confusion matrices generated from the final models trained on the moment decomposition (a) and catch22 (b) datasets.

overview of the classification ability of the tested models. The rows correspond to the peptide predicted by the neural network, whereas the columns correspond to the actual peptide label assigned to the data. Rows in the matrix are normalized by the true labels as to avoid potential bias due to data imbalance. In the ideal case, these matrices have a solid diagonal color and no off-diagonal predictions. In both cases, this holds only for a limited number of peptides, but overall, both methods show strong predictive performance. Table 1 outlines additional metrics for understanding these results further.

Table 1: Classification results of the dense neural networks after training on each feature set. The precision, recall and  $F_1$ -score computed by weighting each class metric by the number of available labels of that class.

Feature set	Balanced accuracy	Precision	Recall	$F_1$ -score
Moment decomposition	0.728	0.731	0.730	0.726
Catch22	0.736	0.737	0.736	0.733

Table 1 show that the catch22 trained model achieved marginally better classification performance than the moment decomposition, although it still failed to discern all peptide ladder classes fully. The precision score, which indicates how often a peptide ladder was cor-

rectly predicted compared to the total number of times it was predicted, is slightly improved in the catch22 model, suggesting a smaller number of false predictions on average. The recall scores show a similar trend, with the catch22 trained models less likely to miss a true classification. Therefore, it is unsurprising that the  $F_1$ -score, comprised of both precision and recall, also follows this trend. This relatively simple analysis method can classify the 42 peptide classes surprisingly well. However, in many of these cases, mean current alone can be used, as outlined in Behrends and Ensslen<sup>25</sup>. Therefore, to highlight the specific role of the higher-order moments, the model capabilities of distinguishing between the six decapeptides is shown in Figure 4. These decapeptides are chosen as they have identical mass, resulting in a high degree of overlap in the event mean histogram, making prediction based on the mean alone infeasible. Specifically, the confusion matrix in Figure 4b shows that identification of the decapeptides can be achieved beyond the straightforward comparison of the mean current of the normalized events, highlighting that additional information lies in higher-order moments of the signal, and supporting the use of more sophisticated classification methods. Note that the histograms in Figure 4a do not represent the optimally achievable identification of the mean current. Rather, the event detection explicitly includes parts of the rising and falling phase in each event, which broadens and possibly skews all peaks. This can be accounted for by employing additional steps in the event preprocessing<sup>21</sup>. For this task however, we explicitly include the rise and fall of each event based on the assumption that they might also contribute to the features in both feature sets.

By demonstrating that we can classify peptides with highly overlapping current signals, we show that in the future, such a method could be used to analyze large samples of peptides without extensive preprocessing, and that perhaps separation of these peptides in a lab setting can also be avoided. This opens not only open new possibilities for scientists performing nanopore experiments, but also provides a means for future investigation into clinical peptide classification applications, where extensive distillation of peptides before classification might be expensive or impractical.

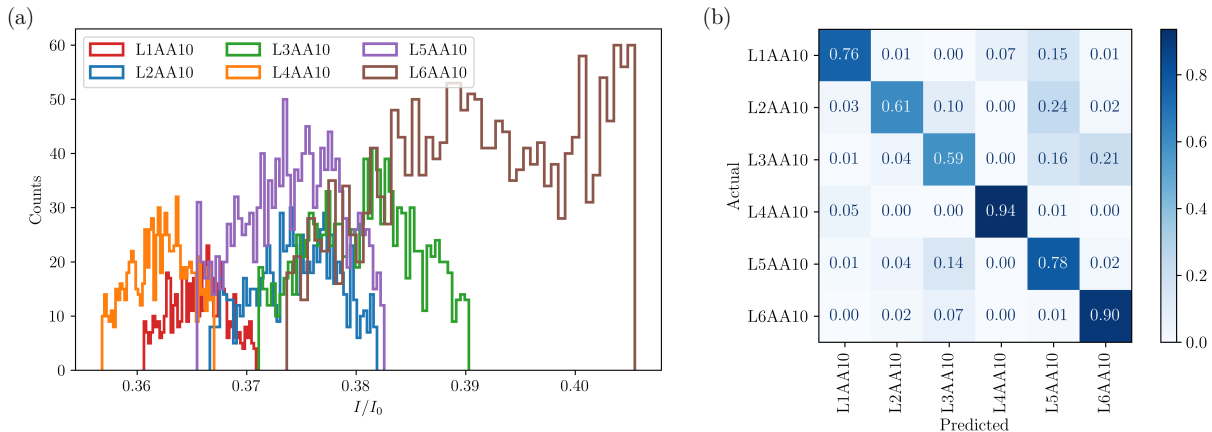


Figure 4: (a) Histogram of the mean blocking currents of the decapeptides of each peptide ladder. Labelling was performed based on an interval only around each peak, which explains the cut sharp edges of all histograms. (b) Model results of the moment decomposition model, tested on the decapeptide samples in the test dataset.

## SHAP Model Explanation

Aside from simplicity, an additional benefit of using the model inputs chosen here is their interpretability. Specifically, the variables being passed to the network are well-defined measurements. By performing SHAP analysis on the trained models, we can thus evaluate the importance of all features in each feature set. The results of this analysis are shown in Figure 5. In a standard SHAP figure, the SHAP value indicates whether the variable increased (positive) or decreased (negative) the model output. The color of each point indicates whether a large (red) or small (blue) scalar value of that feature, the feature value, led to the change. For example, a small feature value with a large SHAP score would indicate that small scalar values for that feature were correlated with larger model outputs. To study the impact of the features with respect to their scalar values, the absolute SHAP values are shown. Examining Figure 5, several interesting outcomes are evident. First, input features present in both datasets, such as the mean blocking current and the logarithmic dwell time, show similar importance characteristics. The catch22-trained models also seemed to depend greatly on the autocorrelation time as estimated by computing the autocorrelation function of an event, indicating that dynamic properties also have an impact on the model prediction.

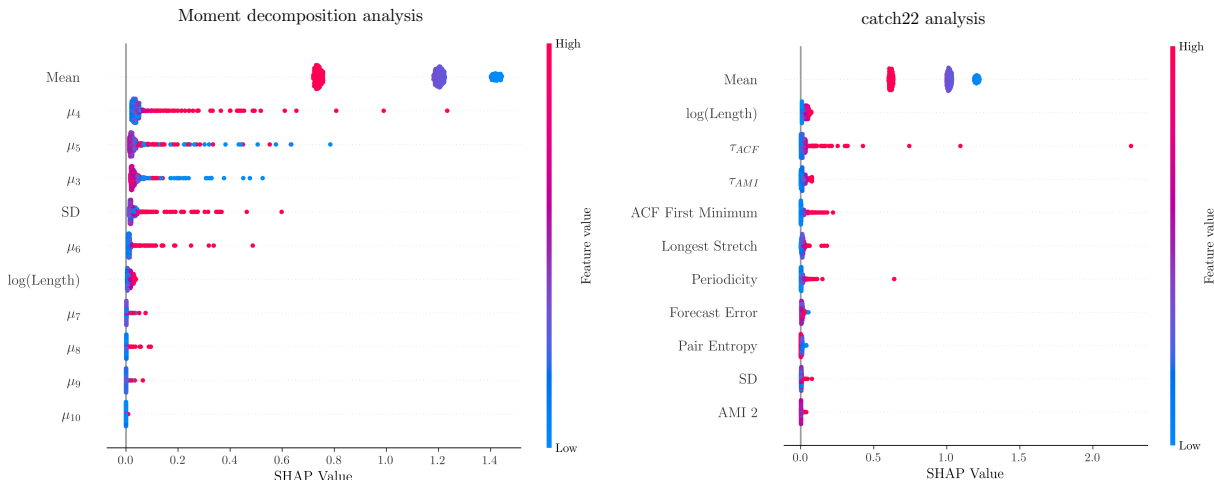


Figure 5: SHAP analysis for both the statistical moments (left) and catch22 (right) computed over all 42 peptides. The top 11 features were taken from both, and the rest fell below statistical significance. A detailed overview of the catch22 features can be found in Table 1 of the supplementary information.

This was completely missed in the statistical moment analysis but might be key to further improvements in predictive performance.

Not taken into account are correlations between features, which was not captured by the SHAP analysis. However, the similarity in importance scores of the inputs present in both datasets suggests that the correlations of inputs are negligible.

## Conclusions

We have demonstrated that the moment decomposition of the time series data generated in nanopore experiments, either through the moments of the distributions formed by the events or more sophisticated analysis with the catch22 feature set, can be used to construct feature vectors for input into classification models. Based on the non-Gaussian form of the histograms, these features capture information present in the higher order moments of the current signal distributions. We showed that using small neural networks, classification accuracies of 72.8 % and 73.6 % can be achieved for the moments and catch22, respectively, with up to 42 peptide classes. These results were emphasized by showing the performance

on the decapeptides where single event distinction is hindered by overlaps in the relative current mean histogram. We further found through SHAP analysis that the signal’s dynamic properties yielded additional classification performance in the catch22 dataset and should be considered in more complex feature decomposition approaches. This simple analysis is computationally efficient and capable of previously unseen classification performance on many classes. Our results highlight the role machine-learning classification can play in classification of large numbers of peptides that may one day be used in a clinical setting. Further, we demonstrate that preparative separation of peptides in experimental settings may not be necessary, as our models can differentiate those with highly overlapping mean blockade currents.

## Methods

### Peptides

In this investigation, we perform classification on 42 peptides, successively constructed by one to six N-terminal amino acids. Figure 6 demonstrates the construction of the 6 individual ladders taken from Behrends and Ensslen<sup>25</sup>. The far left side shows the N-terminus with the

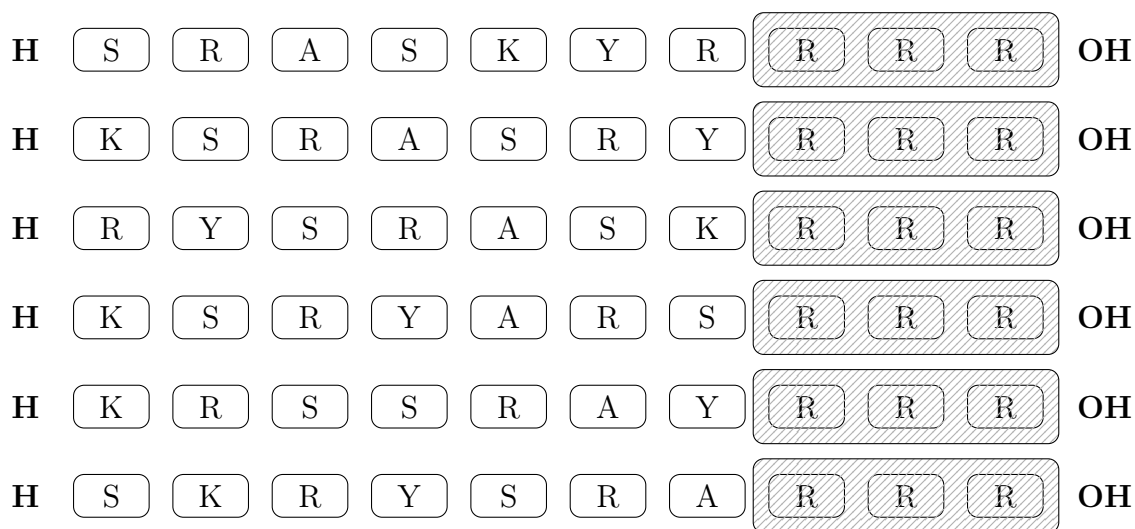


Figure 6: Description of peptide ladders used in the investigation.

hydrogen group, and the far right shows the C terminus with the hydroxide group. Letters S, R, A, K, and Y correspond to the amino acids Serine, Arginine, Alanine, Lysine, and Tyrosine respectively.

## Event Detection and Labeling

During nanopore experiments, a time series of current measurements is captured, within which many events will occur. Before these events can be classified, they must first be isolated from this large sequence. In this work, a statistical threshold detection approach<sup>18,26</sup> was used, wherein deviations from the Gaussian-like distribution of the open pore current are used to detect outliers. If a current was detected below three standard deviations,  $\sigma$ , from the expected open-pore mean current, it was considered the beginning of an event. To avoid unwanted events in the dataset, a wavelet threshold filter using the `bior1.5` with a hard threshold of 0.5 was applied before the detection algorithm, and events whose mean current was above a second threshold of  $4\sigma$  were ignored in line with Piguet *et al.*<sup>26</sup>. Further reduction of spurious events was achieved by only allowing events with a dwell time greater than 80  $\mu$ s. Finally, all detected events were normalized by the mean of the surrounding open pore current. To account for drift in open pore current over time, a consequence of the experimental configuration being used, the mean open pore current was calculated by taking a window around each detected event and ignoring other events that might fall within this window. For labeling, the peaks in the histogram were fitted with Voigt functions. Peptide-specific events were then identified if they fell within the full-width-half-maximum (FWHM) of each peak. Strictly speaking, this discrimination of events for labeling poses a potential source for errors, as neighboring histograms overlap with each other and may, therefore, fall within the FWHM of their neighbor, thus ending up falsely labelled. Since labeling is done using the normalized event mean histogram for all measurements of one specific ladder, there are no labeling errors between peptides with the same amount of amino acids. We therefore expect the amount of data leakage in our approach to be small. The plots used for labelling

can be found in the supporting information.

During data collection, each peptide, along with all of its subchains, are studied in a single experiment. This separation of chains allows for easier labelling as there is less overlap in the current amplitude histograms, an example of which is shown in Figure 7. However, in the classification task, we treat the data as though all 42 peptide chains are being measured together in a single sample, resulting in the amplitude histograms shown in Figure 7 and making the use of more sophisticated machine-learning and statistical feature extraction necessary.

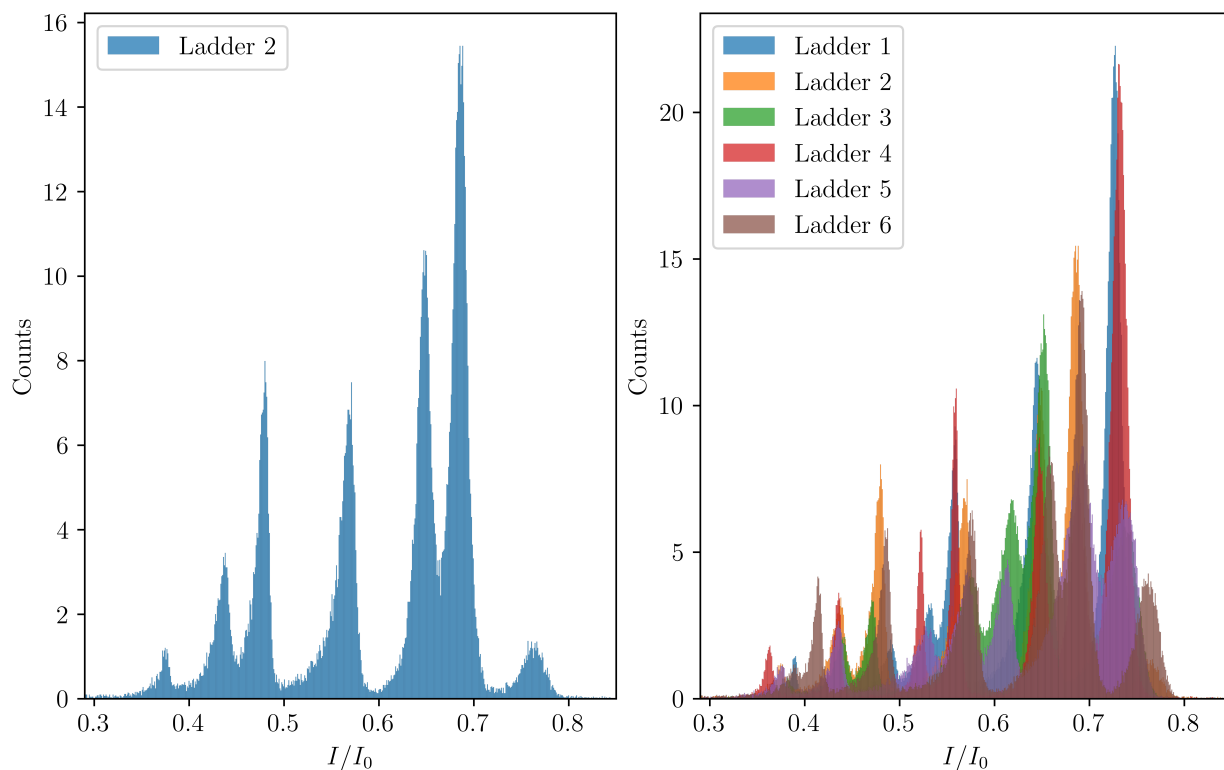


Figure 7: Normalized mean event histograms for all 42 peptides considered in a single experiment. (left) Histogram formed from the normalized event mean of the L2 ladder experiment. (right) Histogram formed from the combined measurements of all 6 ladders.

## Moments Analysis

The  $n^{\text{th}}$  central moment of a random variable,  $X$ , is defined as

$$\mu^n = \langle (X - \mu)^n \rangle = \sum_i (x_i - \mu)^n f(x_i), \quad (1)$$

for probability density  $f$  and mean  $\mu$ .<sup>27</sup> The set of all moments for a distribution can completely define it and comprise a complete or overcomplete representation, making them useful classification problems. In this work, the distribution formed by computing the kernel density estimate<sup>28,29</sup> is used to extract the first ten moments of the distributions of magnitudes of current signals, which form a feature vector for each pore-entry event. The moments themselves were computed using Scipy<sup>30</sup>. In addition to these moments, we also included the natural logarithm of the dwell time of the events in the feature vector, resulting in 11 final features for each event.

## Catch22 Feature Extraction

Another approach to feature extraction performed in this study is using the *catch22* framework from Lubba *et al.*<sup>22</sup> to generate feature vectors. *catch22* is constructed from the larger HCTSA feature extraction toolkit<sup>31,32</sup>, which produces more than seven thousand features of a time series. In their 2019 work, Lubba *et al.*<sup>22</sup> demonstrated that these seven thousand features can be reduced to twenty-two with minimal performance loss when used for classification tasks. The feature extraction is performed in this work using the Python package provided by the initial research group. The extracted features, including the mean current, the standard deviation and the natural logarithm of the dwell time, are used in further analysis.

## SHAP Analysis

SHapley Additive exPlanation (SHAP) analysis<sup>33</sup> is an approach built on game theory to explain how the outputs of a machine learning model are impacted by the inputs, in many ways, explaining what factors in the input data have led to the result. It does so by using the SHAP value, a number that indicates how a certain input value (high or low) impacted the network’s output by either increasing or decreasing it. A large positive SHAP score associated with a large input number indicates that large values of this input increase the network’s output. The same logic carries for negative SHAP values. SHAP analysis can be used to better understand the effect of the neural network inputs on predictive performance. This, in turn, simplifies problems by exposing redundant inputs and illuminates how certain conclusions are reached using the model. This work utilizes the `shap` Python package to analyze the predictions generated by the neural networks.

## Neural Networks

All neural networks were implemented using the PyTorch library<sup>34</sup>. The architectures used in the final model fits are outlined in Table 2 along with their relevant hyperparameters used for the training. These architectures were chosen based on a parameter search over widths from 32 to 512 and depths from 1 to 5.

Table 2: Neural network parameters used in the statistical moments and catch22 dataset training. ReLU activation functions are used between all dense layers, the dimension of which is specified by the superscript. The parameters are trained using the AMSGrad optimizer<sup>35</sup> with a learning rate 0.001.

Architecture	ReLU ( $\mathcal{D}^{64}$ ) ReLU ( $\mathcal{D}^{128}$ ) ReLU ( $\mathcal{D}^{42}$ )
Batch Size	1000
Optimizer	AMSGrad(0.001)
Train Data	242601

## Confusion Matrices

A confusion matrix for multiclass classification is an essential tool for evaluating the performance of a classification model. It visually represents the classifier's predictions compared to the actual classes, with each row corresponding to actual peptide ladder classes and each column to predicted classes. Key metrics such as precision, recall, and F1 score can be derived from the confusion matrix. Precision measures the proportion of true positive predictions among all positive predictions, indicating the model's accuracy in identifying a specific peptide ladder class. Recall, or sensitivity, measures the proportion of true positives among actual positives, reflecting the model's ability to capture all instances of a specific class. The F1 score, the harmonic mean of precision and recall, provides a balanced metric that considers false positives and negatives, making it particularly useful when dealing with imbalanced classes.

## Acknowledgement

This work was supported by the BMBF FKZ 03ZU1208AM: nanodiag BW. The authors of C.H.'s group acknowledge financial support from the German Funding Agency (Deutsche Forschungsgemeinschaft DFG) under Germany's Excellence Strategy EXC 2075-390740016. Partially, this work was also supported by the Deutsche Forschungsgemeinschaft (DFG, German Research Foundation), Project-No 497249646, SPP 2363- "Utilization and Development of Machine Learning for Molecular Applications – Molecular Machine Learning.". Initial work on this project in the lab of JCB was also funded by the BMBF through project ProNanoPep (PTJ 031B1120A).

## Supporting Information Available

The supporting information includes:

- t-SNE plots for different parameters.
- Plots of the fitting process.
- Extended description of the catch22 features.
- Details on the nanopore fabrication and experimental data collection.

## References

1. Wang, Y.; Zhao, Y.; Bollas, A.; Wang, Y.; Au, K. F. Nanopore sequencing technology, bioinformatics and applications. *Nature Biotechnology* **2021**, *39*, 1348–1365.
2. Hoenen, T.; Groseth, A.; Rosenke, K.; Fischer, R. J.; Hoenen, A.; Judson, S. D.; Martel- laro, C.; Falzarano, D.; Marzi, A.; Squires, R. B.; Wollenberg, K. R.; De Wit, E.; Prescott, J.; Safronetz, D.; Van Doremalen, N.; Bushmaker, T.; Feldmann, F.; Mc- Nally, K.; Bolay, F. K.; Fields, B. *et al.* Nanopore Sequencing as a Rapidly Deployable Ebola Outbreak Tool. **2016**, *22*.
3. Kafetzopoulou, L. E.; Pullan, S. T.; Lemey, P.; Suchard, M. A.; Ehichioya, D. U.; Pahlmann, M.; Thielebein, A.; Hinzmann, J.; Oestereich, L.; Wozniak, D. M.; Efthymi- adis, K.; Schachten, D.; Koenig, F.; Matjeschk, J.; Lorenzen, S.; Lumley, S.; Ighodalo, Y.; Adomeh, D. I.; Olokor, T.; Omomoh, E. *et al.* Metagenomic sequencing at the epicenter of the Nigeria 2018 Lassa fever outbreak. **2019**, *363*, 74–77.
4. Jain, M.; Koren, S.; Miga, K. H.; Quick, J.; Rand, A. C.; Sasani, T. A.; Tyson, J. R.; Beggs, A. D.; Dilthey, A. T.; Fiddes, I. T.; Malla, S.; Marriott, H.; Nieto, T.; O’Grady, J.; Olsen, H. E.; Pedersen, B. S.; Rhie, A.; Richardson, H.; Quinlan, A. R.; Snutch, T. P. *et al.* Nanopore sequencing and assembly of a human genome with ultra-long reads. **2018**, *36*, 338–345.

5. Vermeulen, C.; Pagès-Gallego, M.; Kester, L.; Kranendonk, M. E. G.; Wesseling, P.; Verburg, N.; De Witt Hamer, P.; Kooi, E. J.; Dankmeijer, L.; Van Der Lugt, J.; Van Baarsen, K.; Hoving, E. W.; Tops, B. B. J.; De Ridder, J. Ultra-fast deep-learned CNS tumour classification during surgery. **2023**, *622*, 842–849.
6. Hamley, I. W. *Introduction to peptide science*; Wiley, 2020.
7. Díaz Carral, A.; Ostertag, M.; Fyta, M. Deep learning for nanopore ionic current blockades. *The Journal of Chemical Physics* **2021**, *154*, 044111.
8. Bao, Y.; Wadden, J.; Erb-Downward, J. R.; Ranjan, P.; Zhou, W.; McDonald, T. L.; Mills, R. E.; Boyle, A. P.; Dickson, R. P.; Blaauw, D.; Welch, J. D. SquiggleNet: real-time, direct classification of nanopore signals. **2021**, *22*, 298.
9. Senanayake, A.; Gamaarachchi, H.; Herath, D.; Ragel, R. DeepSelectNet: deep neural network based selective sequencing for oxford nanopore sequencing. **2023**, *24*, 31.
10. Wang, K.; Zhang, S.; Zhou, X.; Yang, X.; Li, X.; Wang, Y.; Fan, P.; Xiao, Y.; Sun, W.; Zhang, P.; Li, W.; Huang, S. Unambiguous discrimination of all 20 proteinogenic amino acids and their modifications by nanopore. **2024**, *21*, 92–101, Publisher: Nature Publishing Group.
11. Zhang, Y.; Yi, Y.; Li, Z.; Zhou, K.; Liu, L.; Wu, H.-C. Peptide sequencing based on host–guest interaction-assisted nanopore sensing. **2024**, *21*, 102–109, Publisher: Nature Publishing Group.
12. Li, W.; Li, F.; Zhang, X.; Lin, H.-K.; Xu, C. Insights into the post-translational modification and its emerging role in shaping the tumor microenvironment. *Signal Transduction and Targeted Therapy* **2021**, *6*, 422.
13. Wang, H.; Yang, L.; Liu, M.; Luo, J. Protein post-translational modifications in the regulation of cancer hallmarks. *Cancer Gene Therapy* **2023**, *30*, 529–547.

14. Srivastava, A. K.; Guadagnin, G.; Cappello, P.; Novelli, F. Post-Translational Modifications in Tumor-Associated Antigens as a Platform for Novel Immuno-Oncology Therapies. *Cancers* **2023**, *15*.
15. Dutta, H.; Jain, N. Post-translational modifications and their implications in cancer. *Frontiers in Oncology* **2023**, *13*.
16. Ouldali, H.; Sarthak, K.; Ensslen, T.; Piguet, F.; Manivet, P.; Pelta, J.; Behrends, J. C.; Aksimentiev, A.; Oukhaled, A. Electrical recognition of the twenty proteinogenic amino acids using an aerolysin nanopore. **2020**, *38*, 176–181.
17. Ensslen, T.; Sarthak, K.; Aksimentiev, A.; Behrends, J. C. Resolving Isomeric Post-translational Modifications Using a Biological Nanopore as a Sensor of Molecular Shape. *Journal of the American Chemical Society* **2022**, *144*, 16060–16068, PMID: 36007197.
18. Cao, C.; Magalhães, P.; Krapp, L. F.; Bada Juarez, J. F.; Mayer, S. F.; Rukes, V.; Chiki, A.; Lashuel, H. A.; Dal Peraro, M. Deep Learning-Assisted Single-Molecule Detection of Protein Post-translational Modifications with a Biological Nanopore. *ACS Nano* **2024**, *18*, 1504–1515.
19. Afshar Bakshloo, M.; Kasianowicz, J. J.; Pastoriza-Gallego, M.; Mathé, J.; Daniel, R.; Piguet, F.; Oukhaled, A. Nanopore-Based Protein Identification. **2022**, *144*, 2716–2725.
20. Badrinarayanan, S.; Guntuboina, C.; Mollaei, P.; Farimani, A. B. Multi-Peptide: Multimodality Leveraged Language-Graph Learning of Peptide Properties. 2024; <https://arxiv.org/abs/2407.03380>.
21. Ensslen, T.; Behrends, J. C. To be published. 2024.
22. Lubba, C. H.; Sethi, S. S.; Knaute, P.; Schultz, S. R.; Fulcher, B. D.; Jones, N. S. catch22: CAnonical Time-series CHaracteristics. *Data Mining and Knowledge Discovery* **2019**, *33*, 1821–1852.

23. van der Maaten, L.; Hinton, G. Visualizing Data using t-SNE. *Journal of Machine Learning Research* **2008**, *9*, 2579–2605.
24. Pedregosa, F.; Varoquaux, G.; Gramfort, A.; Michel, V.; Thirion, B.; Grisel, O.; Blondel, M.; Prettenhofer, P.; Weiss, R.; Dubourg, V.; Vanderplas, J.; Passos, A.; Cournapeau, D.; Brucher, M.; Perrot, M.; Duchesnay, E. Scikit-learn: Machine Learning in Python. *Journal of Machine Learning Research* **2011**, *12*, 2825–2830.
25. Behrends, J. C.; Ensslen, T. Method and systems for identifying a sequence of monomer units of a biological or synthetic heteropolymer. Patent US20240077491A1, March 7, 2024.
26. Piguet, F.; Ensslen, T.; Bakshloo, M. A.; Talarimoghari, M.; Ouldali, H.; Baaken, G.; Zaitseva, E.; Pastoriza-Gallego, M.; Behrends, J. C.; Oukhaled, A. In *Pore-Forming Toxins*; Heuck, A. P., Ed.; Methods in Enzymology; Academic Press, 2021; Vol. 649; pp 587–634.
27. Papoulis, A.; Pillai, S. *Probability, Random Variables, and Stochastic Processes*; McGraw-Hill series in electrical and computer engineering; McGraw-Hill, 2002.
28. Rosenblatt, M. Remarks on Some Nonparametric Estimates of a Density Function. *The Annals of Mathematical Statistics* **1956**, *27*, 832 – 837.
29. Parzen, E. On Estimation of a Probability Density Function and Mode. *The Annals of Mathematical Statistics* **1962**, *33*, 1065 – 1076.
30. Virtanen, P.; Gommers, R.; Oliphant, T. E.; Haberland, M.; Reddy, T.; Cournapeau, D.; Burovski, E.; Peterson, P.; Weckesser, W.; Bright, J.; van der Walt, S. J.; Brett, M.; Wilson, J.; Millman, K. J.; Mayorov, N.; Nelson, A. R. J.; Jones, E.; Kern, R.; Larson, E.; Carey, C. J. *et al.* SciPy 1.0: Fundamental Algorithms for Scientific Computing in Python. *Nature Methods* **2020**, *17*, 261–272.

31. Fulcher, B. D.; Little, M. A.; Jones, N. S. Highly comparative time-series analysis: the empirical structure of time series and their methods. *Journal of The Royal Society Interface* **2013**, *10*, 20130048.
32. Fulcher, B. D.; Jones, N. S. hctsa: A Computational Framework for Automated Time-Series Phenotyping Using Massive Feature Extraction. *Cell Systems* **2017**, *5*, 527–531.e3.
33. Lundberg, S. M.; Lee, S.-I. A unified approach to interpreting model predictions. Proceedings of the 31st International Conference on Neural Information Processing Systems. Red Hook, NY, USA, 2017; p 4768–4777.
34. Paszke, A.; Gross, S.; Massa, F.; Lerer, A.; Bradbury, J.; Chanan, G.; Killeen, T.; Lin, Z.; Gimelshein, N.; Antiga, L.; Desmaison, A.; Köpf, A.; Yang, E.; DeVito, Z.; Raison, M.; Tejani, A.; Chilamkurthy, S.; Steiner, B.; Fang, L.; Bai, J. *et al.* PyTorch: An Imperative Style, High-Performance Deep Learning Library. 2019.
35. Reddi, S. J.; Kale, S.; Kumar, S. On the Convergence of Adam and Beyond. *CoRR* **2019**, *abs/1904.09237*.